Applied Physics B (2020) 126:6
https://doi.org/10.1007/s00340-019-7350-5

Applied Physics B
Lasers and Optics

Particulate emissions measurements by laser-based techniques in a boiler fueled by wood pellets

Salma Bejaoui[1] · Marie Creyx[2] · Eric Delacourt[2] · Céline Morin[2] · Eric Therssen[1]

Received: 24 January 2019 / Accepted: 15 November 2019 / Published online: 2 December 2019

Abstract
This paper describes mainly laser-based techniques applied to a boiler fueled by wood pellets which is a real complicated combustion system. To our knowledge, laser-induced incandescence (LII) and extinction are used to characterize particulate emission at the exhaust for the first time because laser diagnostics are generally applied to laboratory flames, automotive engines and aeroengines. The 30-kW boiler was first characterized by temperature mapping in the combustion chamber and particle diameter analysis by scanning mobility particle sizer at the exhaust and inside the first combustion chamber for a better understanding of the running of this complex combustion system. Non-intrusive laser-based diagnostics including broadband LII, two-color LII and laser extinction excited at 1064 nm have been employed to study the particulate emissions at the exhaust of the boiler during the start-up and the steady-state phases of the boiler. The cross analysis of the experimental results obtained with the different diagnostics shows that particle size distributions, particles volume fractions and the temperature distribution are strongly dependent on the boiler cycle linked to the pellets loading. Laser extinction and LII-based methods provided complementary information about the particulate emissions. The LII technique probes incandescent soot particles formed during the combustion of pellets, while laser extinction detects both soot and non-incandescent particles (such as dust, fly ashes).

1 Introduction

Due to the continuous decrease in the amount and the availability of the conventional fossil fuels, it is becoming inevitable to search for new energy sources. Biomass energy is considered as an attractive option because of many economic and environmental benefits such as reducing the agro-industrial waste, providing energy security, and promoting economic development. Moreover biomass provides renewable energy and has a close to 'carbon neutral' balance since the growing the biomass plants removes as much CO_2 as the amount released to the atmosphere from its combustion. Bioenergy can realistically substitute fossil-based fuel in many types of applications. Biomass combustion already contributes significantly to world energy provision. It provided approximately 14% of the world's energy consumption and 59.2% of the world's energy supply of renewables in 2014 [1]. Among the available renewable energy sources, biomass is the third largest electricity-generating source and the first renewable source in the heating sector [1]. Replacing fossil fuel with a 'carbon-neutral' energy source is one approach to mitigate the increases in atmospheric CO_2 and reduce the greenhouse gas emissions. The case of biomass energy has been widely debated and many concerns have been raised regarding the impact of biomass combustion on human health and air quality. Beside the differing views on the carbon neutrality of biomass energy, its environmental benefits have been questioned as well [2–6]. Biomass burning releases a number of gaseous pollutants such as carbon monoxide, nitrogen oxides (NO_x), volatile organic compounds (VOCs) and polycyclic aromatic hydrocarbons (PAHs) [7–11]. Particulate matter (PM) emission is one of the major concerns of biomass combustion because of its detrimental effect on both human health and environment [5, 6, 9, 11, 12]. Biomass burning generates both large fly ash particles (diameter higher than 1 μm) and fine carbonaceous

This article is part of topical collection of on Laser-Induced Incandescence (Klaus Peter Geigle and Stefan Will).

✉ Eric Therssen
eric.therssen@univ-lille.fr

[1] Faculté des Sciences et Technologies, Université de Lille, 59655 Villeneuve d'Ascq, France

[2] Univ. Polytechnique Hauts-de-France, CNRS, UMR 8201-LAMIH, 59313 Valenciennes, France

particles (diameter lower than 1 µm) that contain ashes as well and soot particles formed under locally fuel-rich conditions [4, 6]. Many investigations have been performed recently to study PM formation and emissions from solid biomass fired combustors to help assess its impact on human health and climate change [10, 11, 13, 14]. Experimental studies have reported the PM concentrations and size distributions in domestic biomass boiler and analyzed the impact of several factors such as the operational conditions, the operational load, the combustor design, the air excess and the biomass compositions [9, 13–15]. These studies concluded that biomass combustion can be optimized to reduce the particulate emission by improving the combustor design, extending combustion times and enhancing the combustion efficiency. The aim of this study is to investigate experimentally the particulate pollutant emission from a boiler fueled by wood pellets with a nominal thermal capacity of 30 kW used for domestic heating. This boiler is equipped with an oxygen sensor that automatically controls the air excess and a secondary combustion chamber to optimize the combustion efficiency and reduce particulate emission resulting from the incomplete combustion in the first combustion chamber. To the best of our knowledge, laser-based diagnostics have not been applied for the in situ analysis of PM emissions in biomass-fueled boiler. Here, we apply the broadband laser-induced incandescence (LII), the two-color LII, and laser extinction to detect in real time the particulate emissions (nanoparticles of soot, fly ashes) at the exhaust of the test bench. Additional ex situ measurements using a set of thermocouples and a scanning mobility particle sizer (SMPS) have been performed to derive the temperature distributions and the PM size distributions. All these measurements have been performed in the start-up, transient and steady-state phases to study the impact on the PM emissions of the residential pellet boiler. The paper is presented as follows: the description of the boiler fueled by wood pellets used in our experiments, the temperature and the particles size distributions measurements are presented in Sect. 2. The methodology and the experimental setups of the laser-based techniques including the broadband LII, the two-color LII and the laser extinction are described in Sect. 3. The experimental results are presented and discussed in Sect. 4 followed by the conclusion in Sect. 5.

2 Description of the test bench

2.1 The domestic boiler fueled by wood pellets

The experiments are carried out in a domestic 30-kW boiler fueled by wood pellets (Fig. 1a). The pellets are supplied in the fixed bed furnace by a screw conveyor equipped with a magnetic sensor. This sensor measures the angular rotation of the screw and thus periods and the mass of pellets introduced into the first combustion chamber (the furnace). The boiler is equipped with an oxygen sensor, also called

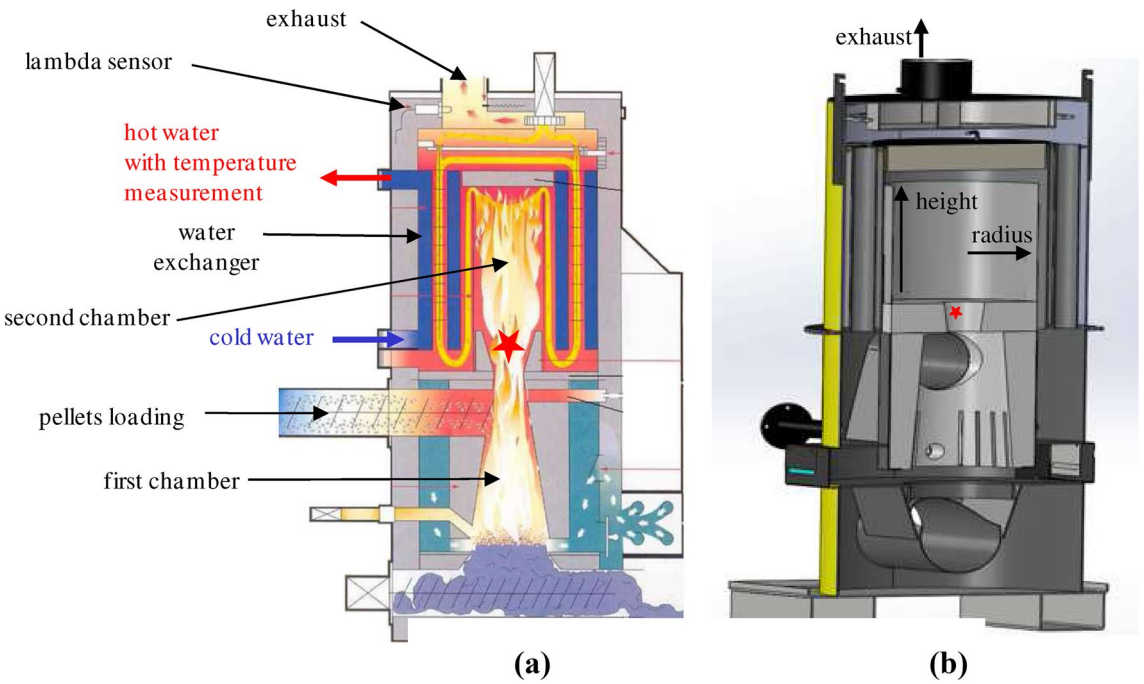

Fig. 1 **a** Schematic picture of the 30-kW boiler fueled by wood pellets, **b** 3D picture of the boiler with coordinates (radius and height) defined in second combustion chamber, red star: aperture between the two chambers

Lambda sensor that measures the residual oxygen content in the exhaust gases and automatically adjust the air excess factor according to the operating conditions. Above the first combustion chamber, the hot gases and particles emitted by the incomplete combustion enter in a second combustion chamber through a 15 cm circular aperture (shown by the red star) in a refractory wall separating the two chambers (Fig. 1b). The second combustion chamber is constituted by a vertical refractory steel cylinder (radius of 18 cm, height of 37 cm) that increases the residence time of unburnt species in a high temperature area to enhance the combustion efficiency. The burned gases exit the second combustion through the exchange zone to heat the water circulating in the boiler. The water temperature is measured by the boiler regulation system at the exit of the heat exchanger (Fig. 1a).

2.2 Particle size measurements

The particles size distributions are measured using a nanoparticle-size spectrometer (nano-ID NPS 500) also called SMPS with a sensitivity range between 5 and 500 nm. The samples are extracted from the first chamber (furnace) and from the exhaust of the boiler using a stainless steel 1/4-in. outer diameter probe. The measurements are performed during the start-up and the steady-state phases.

2.3 Temperature measurements of the flue gas

The flue gas temperatures are measured using a set of 6 S-type thermocouples with 0.2-mm diameter positioned at several vertical and radial positions in the second chamber (Fig. 2). A 0.13-mm-diameter S-type thermocouple is also used to estimate the radiative heat losses from the bead of the thermocouples [16]. With a temperature of 600 °C, the correction is estimated to 44 °C and can reach 187 °C for a flue gas measured temperature of 1000 °C (mainly because of the hot junction radiative losses).

The signal related to the angular rotation of the screw conveyor and thus to the pellets loading is recorded simultaneously with gas temperature at the top of the second chamber (Fig. 3). At the nominal operational condition, the pellets are introduced during 3 s with a 24-s interval between two pellets loads. When the hot water temperature is lower than its set point, the screw conveyor of pellets performs rotation cycles to supply the first chamber (furnace). When the set point is reached, the screw conveyor cycles are stopped until the hot water temperature becomes again lower than its set point. This regulation reveals a thermal cycle as shown in Fig. 3.

The thermal cycles start during the steady regime (see after Fig. 8c). The boiler works with a thermal cycle of 12 min; this period is from the beginning of gas temperature decrease at the top of the second chamber (radius = 9 cm and height = 33 cm) to the end of the feeding time (Fig. 3).

The temperatures of flue gas measured at different radial (from 7 to 17 cm) and vertical (from 8 to 36 cm) positions in the second chamber are presented in Fig. 4 for nine instants

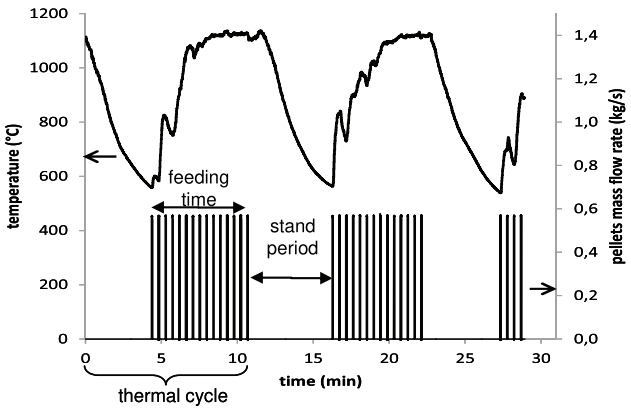

Fig. 3 Gas temperature at the top of the second chamber (radius = 9 cm and height = 33 cm) and the mass flow rate of pellets during two boiler cycles

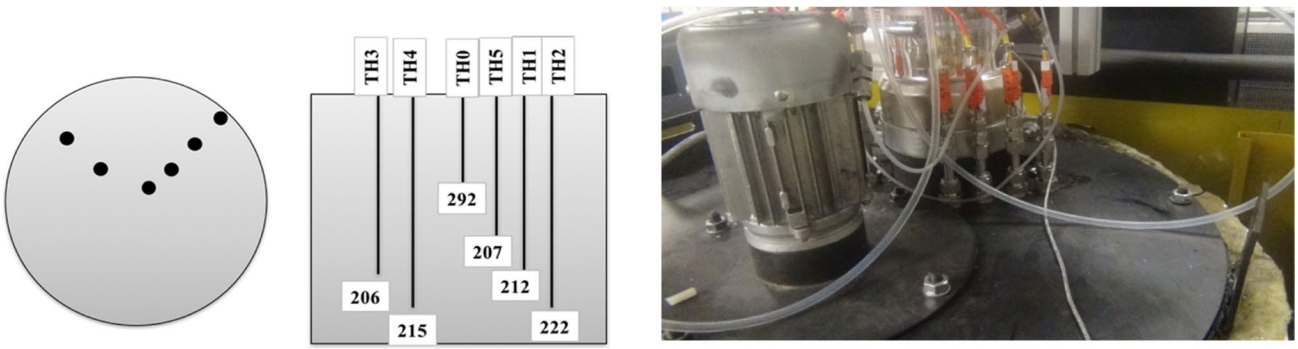

Fig. 2 Right: image of the thermocouples inserted from the top of the boiler in the second chamber. Center: front view of radial position and example of thermocouples heights (given in mm). Left: top view of radial position of the thermocouples

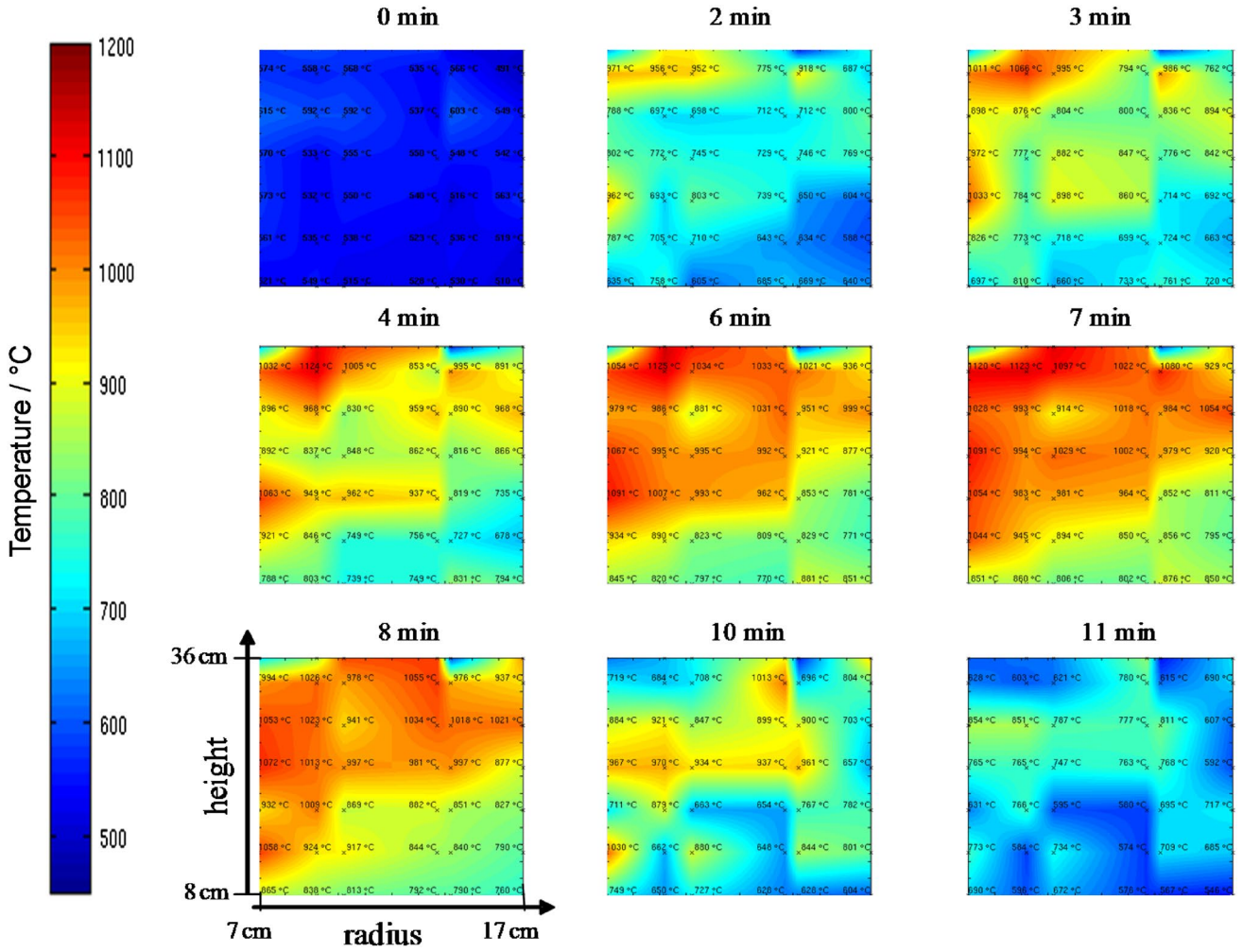

Fig. 4 During the steady regime, several radial and vertical positions of thermocouple measurements (symbol: cross) are presented into the second chamber at nine instants of the thermal cycle. Temperature mapping (with a color scale in °C shown at the left of the figure) was obtained by linear interpolation. The horizontal axis corresponds to the radius (from 7 to 17 cm) and the vertical axis to the height (from 8 to 36 cm) of the second chamber (also shown in Fig. 1b)

of the boiler working cycle during the steady regime. The positions (represented by crosses) and the measured temperatures (in °C) are represented on the map. A linear interpolation was used to map the temperature field in this chamber.

Considering the cyclic running of the boiler, the flue gas temperatures in the second combustion chamber increase when pellets are supplied in the furnace and decrease when the screw conveyor stops. At the beginning of the boiler thermal cycle, the flue gas temperature is minimal (500–600 °C) and the radial and axial gradients are both uniform.

The temperature increases when the pellets are introduced and reaches its maximal values at mid-cycle (1000–1125 °C). The highest temperatures and thermal gradients are located radially near the central position and vertically near the center and the top of the second combustion chamber. The radial distribution of the temperature remains more uniform than the axial one. The flue gas introduced into the second chamber are heated via thermal radiation and reached higher temperature at the top of this chamber which enhances the thermal efficiency of the boiler.

At the end of the cycle, the temperature and the temperature gradient of the flue gas decrease again and reach values close to the beginning of the cycle (600–730 °C).

3 Laser-based diagnostics

3.1 Laser-induced incandescence (LII)

3.1.1 Principle

Laser-induced incandescence is a highly sensitive diagnostic based on the fast heating of particles with a pulsed laser and observe the subsequent thermal radiation, whilst

the particle cools in a constant pressure and temperature medium. The subsequent isotropic radiation is proportional to the blackbody emission modified by the spectral emissivity of the particles. This radiation also called the LII signal and noted LII (λ, t) can be expressed according to the soot volume fraction f_v (t) over the spectral range $\Delta\lambda = \lambda_f - \lambda_i$ as follows:

$$\mathrm{LII}(\lambda,t) = 24\pi \int_{\lambda_i}^{\lambda_f} \frac{C_1}{\lambda^6} \cdot E(m,\lambda).\left[\exp\left(\frac{C_2}{\lambda.T_p(t)}\right) - 1\right]^{-1} \cdot f_v(t) \cdot \mathrm{d}\lambda, \quad (1)$$

where $C_1 = 2\pi hc^2$ and $C_2 = hc/k$ (h, c, and k are, respectively, the Planck constant, the speed of light and the Boltzmann constant).

Experimentally and theoretically, prompt LII signal has been shown to be proportional to the soot volume fraction [17, 18]. The laser energy, its temporal and spatial distribution and the soot refractive index function $E(m, \lambda)$ are sensitive parameters influencing the energy absorbed by the particle and its temperature. Absolute soot volume fraction can be obtained through auto-compensating procedure based on the detection of the LII signal at least in two or more spectral regions also named 2C-LII [19, 20] or using independent calibration method based on gravimetric or light extinction techniques [21]. For optical-based techniques, the knowledge of the refractive index function $E(m, \lambda)$ is necessary. Some references commonly used to determine $E(m, \lambda)$ are available in [22]. Particularly, many investigations were performed to provide an accurate value of $E(m)$ at 1064 nm. $E(m, 1064\ \mathrm{nm})$ is considered as a reference because at this wavelength, PAHs are transparent which avoids the interference of LII signal with PAH fluorescence.

A low laser energy is employed for soot volume fraction measurements to avoid a phase change of soot particle that could occur at high laser energy [23] and could have an impact on $E(m)$.

3.1.2 Broadband LII experimental setup

Three optical accesses (Fig. 5) are implemented in the chimney with 120-mm diameter to allow laser-based diagnostics. A 10-Hz-pulsed Nd–YAG laser [Big Sky, Quantel CFR 200, full width at half maximum (FWHM) = 5 ns] is used to probe soot particles in the exhaust of the boiler through two circular quartz windows (20 mm). The LII signal emitted from the center of the chimney is detected perpendicularly to the laser propagation through a rectangular quartz window. A broadband detection of LII radiation (named broadband LII in the following) is performed using a set of two achromatic lenses with 200-mm and 150-mm focal lengths focusing the light onto a photomultiplier tube (PMT, Philips XP2237). A LabVIEW program has been developed to record and save the LII data simultaneously with the signal relative to the pellets loading and the 6 thermocouples measurements.

3.2 Two-color laser-induced incandescence (2C-LII)

3.2.1 Principle

The two-color LII (2C-LII) is developed by Snelling et al. [19] to measure the absolute soot volume fraction and the maximum particles temperature reached during the laser pulse. In this approach, the incandescence decay time is measured using two different wavelength detection regions. It is recommended to select the detection regions above 500 nm to avoid the variation of $E(m)$ versus wavelengths [24]. Previous investigations of $E(m, \lambda)/E(m, 1064\ \mathrm{nm})$ in different flames fueled with gas and liquid hydrocarbons show that the extinction properties of soot are relatively independent of fuel type and that the $E(m)$ ratio is constant between 530 and 1064 nm [24–28]. In the present work, detection regions centered on 530 and 700 nm are selected to apply the 2C-LII and derive the absolute soot volume fraction. LII measurements have been carried out using

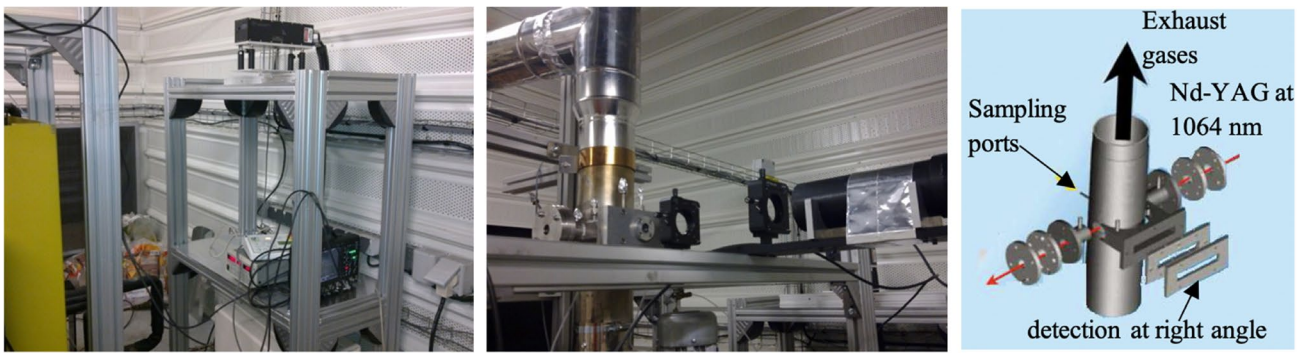

Fig. 5 Left and center: pictures of the LII experimental setup, right: the chimney equipped with three optical accesses for optical diagnostics and a sampling port for SMPS analysis

laser energy (adjusted to 0.15 J/cm^2) under the sublimation threshold to avoid any phase change [23].

Assuming that $\exp(C_2/(\lambda \cdot T_p(t))) \gg 1$ in Eq. (1), the LII signal S_{LII} (λ_i, t) detected in a narrow spectral region $\Delta\lambda_i$ centered on λ_i can be written as:

$$S_{LII}(\lambda_i, t) = 24\pi \cdot \frac{C_1}{\lambda_i^6} \cdot \beta(\lambda_i) \cdot E(m, \lambda_i) \exp\left(-\frac{C_2}{\lambda_i \cdot T_p(t)}\right) \cdot f_v(t) \cdot \Delta\lambda_i, \quad (2)$$

where $\beta(\lambda_i)$ is the detection efficiency of the experimental setup in the region $\Delta\lambda_i$ measured using an integrating sphere (SphereOptics) with a calibrated, uniform, thermal controlled blackbody-like radiation. The radiation emitted by the sphere $S_L(T_L, \lambda_i)$ and detected with the same LII setup can be expressed as:

$$S_L(T_L, \lambda_i) = \frac{C_1}{\lambda_i^5} \cdot \beta(\lambda_i) \cdot \varepsilon_L(\lambda_i) \exp\left(-\frac{C_2}{\lambda_i \cdot T_L}\right) \cdot \Delta\lambda_i, \quad (3)$$

where $\varepsilon_L(\lambda_i)$ is the emissivity of the sphere (given at 0.994) and T_L is the blackbody temperature.

The maximum particles temperature T_p reached during the laser pulse is derived from the ratio of the LII signals in the two spectral regions (Eq. 4), while the absolute soot volume fraction f_v is obtained from the ratio of the LII signal and the sphere radiation in a selected spectral region (Eq. 5):

$$T_p = C_2\left(\frac{1}{\lambda_2} - \frac{1}{\lambda_1}\right)\left[\mathrm{Ln}\left(\frac{S_{LII}(\lambda_1, t)}{S_{LII}(\lambda_2, t)}\right) \cdot \frac{\beta(\lambda_2)}{\beta(\lambda_1)} \cdot \frac{\lambda_1^6}{\lambda_2^6} \cdot \frac{\Delta\lambda_2}{\Delta\lambda_1}\right]^{-1}, \quad (4)$$

$$f_v = \frac{S_{LII}(T_p, \lambda_1)}{S_L(T_L, \lambda_1)} \cdot \frac{\varepsilon_L(\lambda_1) \cdot \lambda_1}{24\pi E(m)} \exp\left[-\frac{C_2}{\lambda_1}\left(\frac{1}{T_p} - \frac{1}{T_L}\right)\right]. \quad (5)$$

3.2.2 The 2C-LII experimental setup

The same excitation setup as for the broadband LII signal is used for the 2C-LII experiment. The detection system is composed by a set of two achromatic lenses ($f_1 = 200$ mm, $f_2 = 150$ mm) and an optical fiber collimator that collimates the emitted light into an optical fiber (200-µm core). The fiber is connected to a Hamamatsu block customized for a dual-wavelength detection (Fig. 6). This block contains a dichroic mirror that transmits wavelengths above 625 nm and reflects light below this wavelength. Two filter blocks centered at 530 and 700 nm with 40 and 60 nm FWHMs, respectively, are placed in front of two identical photomultiplier tubes (PMT-20, Hamamatsu factory) to record the LII signal. As mentioned above, the detection efficiency ratio (required for Eq. 4) is obtained by recording the radiation of the integration sphere in the two spectral regions using the same 2C-LII setup. The temperature T_L of the blackbody radiation is adjusted with a power supply and measured with a calibrated spectrograph linked to the sphere. For these measurements, the temperature T_L is fixed at 3074 K.

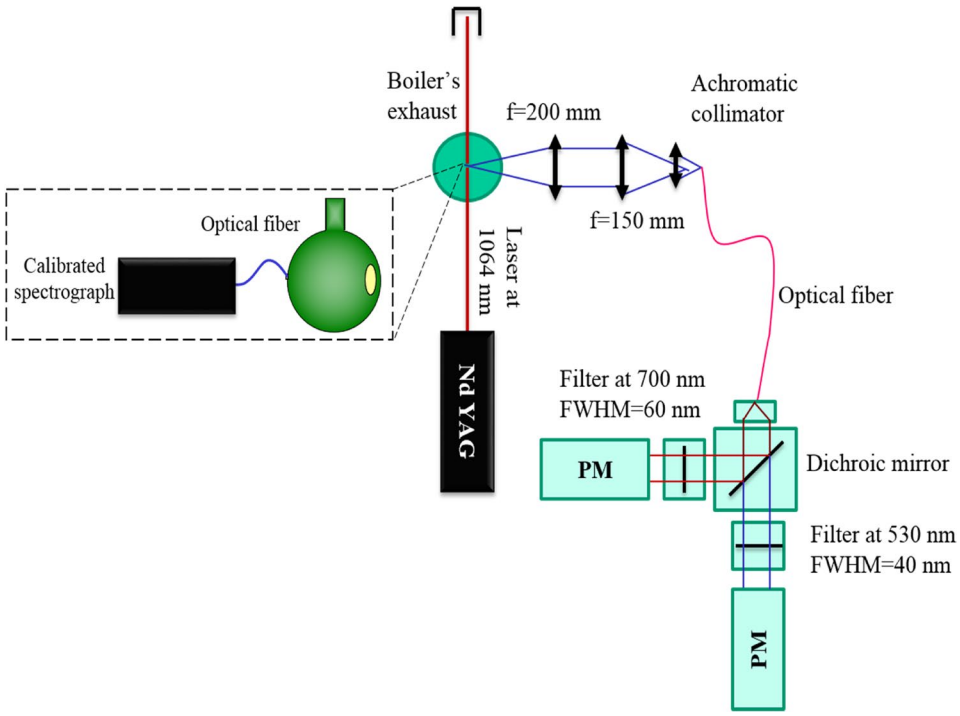

Fig. 6 The two-color LII experimental setup

3.3 Laser extinction

3.3.1 Principle

The laser extinction technique has been widely applied to quantify the particulate carbonaceous pollutants in different experimental apparatuses [29]. This technique consists in measuring the ratio of the incident (I_0) and transmitted light (I) expressed by the Beer–Lambert law (6) as:

$$\frac{I}{I_0} = \exp(-K_{\text{ext}} \cdot L), \tag{6}$$

where L is the path length and K_{ext} is the dimensionless extinction coefficient. The extinction of a laser beam at $\lambda = 1064$ nm in sooting environment is primarily caused by the absorption and the scattering of light (Rayleigh/Mie scattering) by particles. In this work, we assume that the light extinction due to the scattering is negligible based on the SMPS measurements of particles size distributions in the exhaust of the boiler (see Sect. 4.1). Hence, the extinction ratio can be correlated with the concentration of absorbent particles as:

$$\ln\left(\frac{I}{I_0}\right) = -\frac{6\pi E(m,\lambda)}{\lambda} \cdot f_v \cdot L. \tag{7}$$

3.3.2 Extinction experimental setup

Laser extinction measurements are performed using a continuous laser at 1064 nm (laser 2000, 100 mW) injected in the exhaust of the boiler through the two circular quartz windows. The transmitted light and a portion of the incident light reflected by a beam-splitter are detected using two low-noise trans-impedance amplifiers (PDA) (Fig. 7). Laser extinction measurements are coupled with broadband LII measurements using the same experimental setup presented in Sect. 3.1.2. The signal related to the incident and the transmitted laser, the LII decay time and the signal relative to the pellets loading are recorded simultaneously using a LabVIEW program.

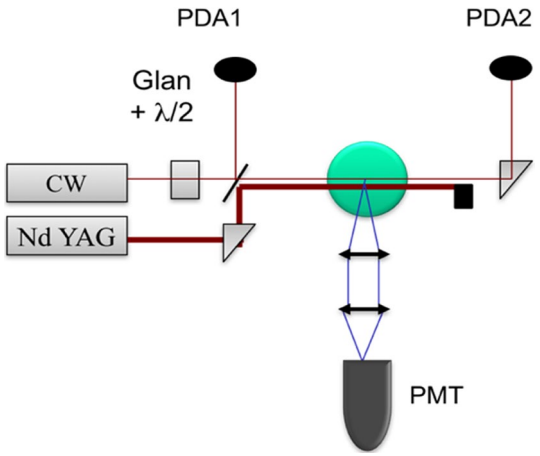

Fig. 7 Experimental setup of the simultaneous laser extinction and broadband LII measurements

4 Results and discussion

4.1 Particle size measurements using SMPS

The particles size distributions (D_p being the mobility diameter of particle) are measured using a nanoparticle-size spectrometer (nano-ID NPS 500) with a sensitivity range between 5 and 500 nm. The samples are extracted from the first combustion chamber and from the exhaust of the boiler. The measurements in the exhaust are performed during the start-up and the steady-state phases of the boiler. The size distributions of solid particles extracted from the exhaust and from the first combustion chamber are presented in Fig. 8a, b, respectively. The size distribution measurements in the exhaust are labeled alphabetically and highlighted in Fig. 8c. The signal related to the angular rotation of the screw conveyor and, thus, to the pellets loading is recorded simultaneously with water temperature. This signal is not shown for clarity but used to interpret the operating regimes of the boiler. The boiler is working at nominal conditions where the pellets are introduced during 3 s with a 24 s interval between two pellets loads. In the start-up phase, the water temperature is lower than the set-point (65 °C) and the pellets load cycle [feeding time, stand period (Fig. 3)] is repeated continuously during the first 50 min. The mean diameter of particles probed in this phase is minimal (lower than 10 nm) and the bimodal size distribution is dominated by the small-size mode (point *A*). At the end of the start-up phase, the water temperature increases rapidly from 30 to 60 °C. A transition phase observed from $t = 50$ min to 2 h shows a slow increase of the water temperature and a fast growth of particles diameter. The pellets loading cycle is also repeated continuously during this phase and the size distributions show a bimodal structure dominated by the large-size mode (points *B*, *C* and *D*). Finally, the boiler reaches the steady state after 2 h and a periodic thermal cycle is established. During a period of this cycle (12 min), the water temperature increase is correlated with the automatic pellets loading, while no pellets are introduced during the decrease of the temperature. The combustion efficiency is optimized in the steady regime and the particles diameters show lower values compared to the transition phase. SMPS measurements in the first combustion chamber during the steady state (Fig. 8b) show a set of three monodisperse size

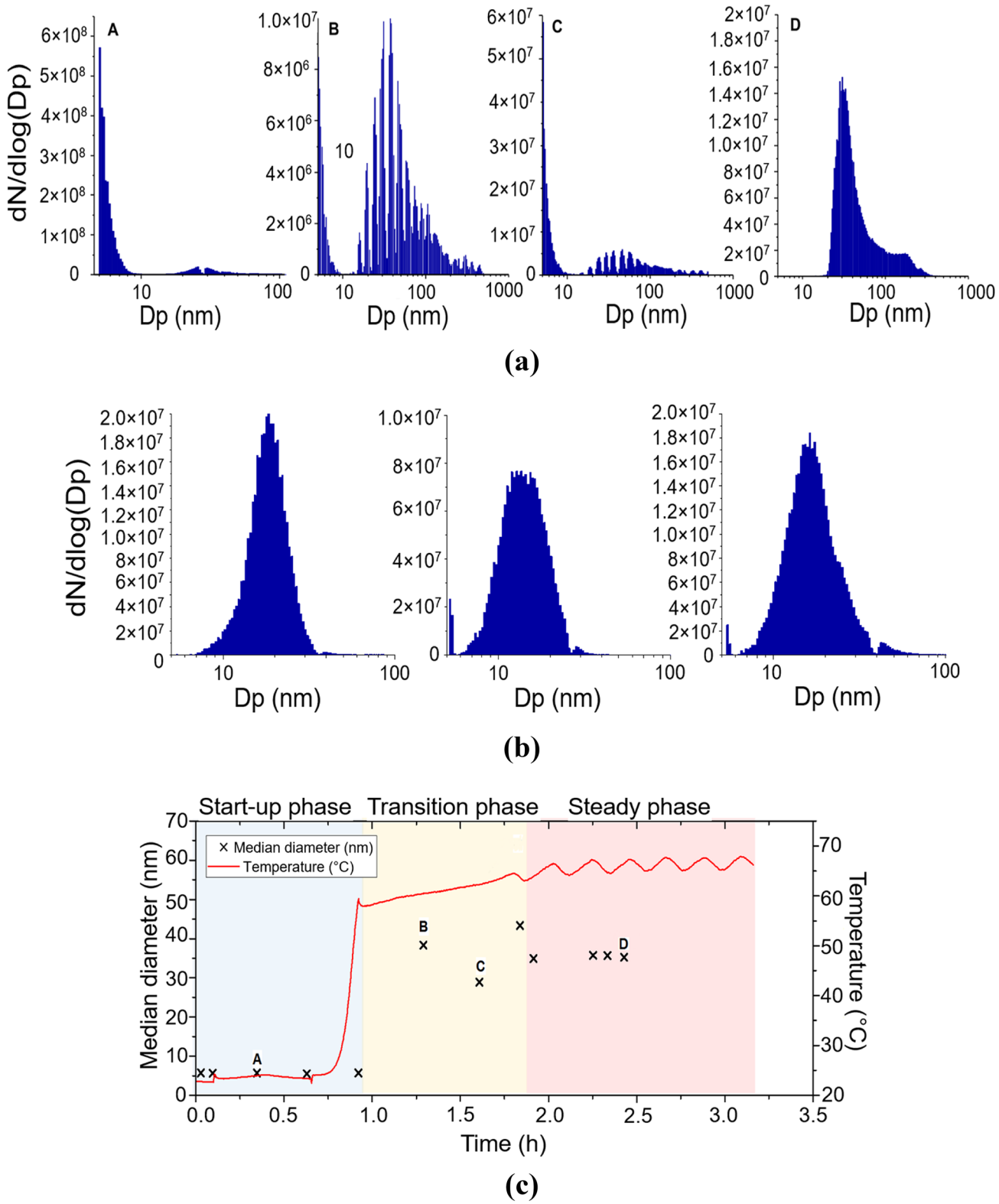

Fig. 8 **a** Size distributions of particles extracted from the exhaust (A: start-up phase; B, C: transition phase; and D: steady state), **b** three size distributions of particles extracted from the first chamber (furnace) of the boiler during the steady state, **c** median diameter of particles probed in the boiler exhaust and the water temperature versus time

distributions with a mean diameter of particles varying from 7 up to 20 nm. Surface growth, coagulation and agglomerations processes occur from the first combustion chamber to the exhaust where the median size of particles is around 35 nm.

4.2 LII signal and soot volume fraction

Here after, the LII results come from different campaigns and are represented differently due to the sampling intervals. We present in Fig. 9 the maximum of broadband LII signal which is very sensitive to the presence of soot nanoparticles because of the large LII detection range, i.e., over some hundreds nanometers. The LII signals versus time (black line) are recorded simultaneously with a binary signal related to the pellets loading in the first combustion chamber (red line) (0: no pellets; 1: pellets are fed in this chamber). Water temperature (blue stars) is presented in the same plot to define the start-up and steady phases. Consistent with the SMPS results, low intensities of LII signals are measured during the start-up phase (up to around 1 h). Soot particles have small diameters and probably low concentrations in this phase.

High intensities of LII signals are observed after 1 h from the ignition. Once the thermal cycle is established, LII emission shows also periodic cycles and the maximum of LII emission occurs during or after the loading of pellets introduced in the first combustion chamber. Indeed, the introduced pellets are heated in contact with the ember bed up to their ignition temperature. Their incomplete combustion produces different unburned species including soot nanoparticles.

In Fig. 10, the local measurements of soot volume fraction obtained with the 2C-LII technique and the signal related to the pellets loading are plotted versus time. In this study, an $E(m)$ value of 0.4 is chosen to well represent mature soot in the exhaust of the boiler [30]. No soot is detected during the start-up regime, while a periodic soot emission is observed when the boiler reaches the steady state. The obtained results show that the maximum soot emission is around 160 ppb. We should note that these measurements represent a local soot concentration detected in small volume of measurement

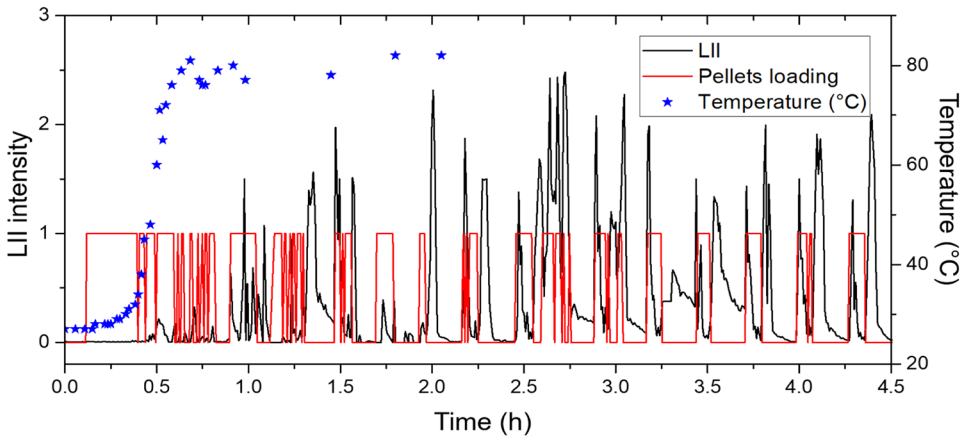

Fig. 9 Maximal intensities of broadband LII (black line) measured simultaneously with the signal related to the pellets loading (red line). The water temperatures are presented to define the start-up and steady regimes (blue stars)

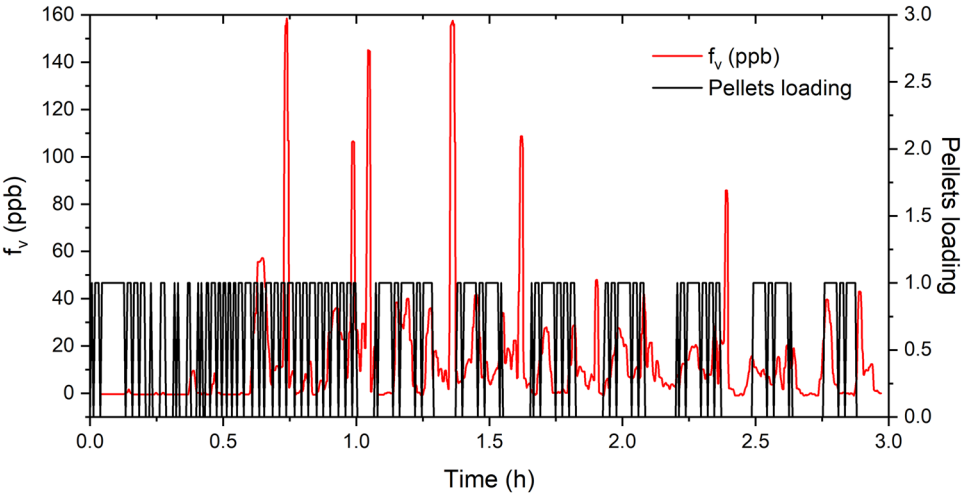

Fig. 10 Soot volume fraction obtained with the 2C-LII technique (red line) measured simultaneously with the signal related to the pellet loadings (black line) versus time

defined by the laser beam diameter and the collection solid angle of the optics. We assume that the radial distribution of the soot volume fraction is uniform at the exhaust but in further experiments, one should take advantages of a camera to map instantaneously the soot along the entire diameter of the exhaust.

4.3 Comparison between LII and laser extinction technique

Particles volume fraction, broadband LII signal (a new series of measurement compared to Fig. 9) and water temperature are reported in Fig. 11 as a function of time. Particles volume fraction is obtained by measuring the extinction of a continuous laser beam at 1064 nm intercepting the exhaust of the boiler and by neglecting (for this first attempt in a biomass boiler) the scattering (according to Eq. 7). LII signals are recorded simultaneously with the extinction measurements using a pulsed laser also at 1064 nm and a broadband detection (setup described in Fig. 7). Comparing LII signals emitted by incandescent soot particles to the extinction signal induced by solid particles (dust, soot, fly ashes, etc.) provide additional information about the nature of the solid particles in the boiler exhaust.

Here, $E(m)$ has been selected at 0.4 as for mature particles [30] to estimate the volume fraction of all the particles. Results show that the light extinction increases gradually during the startup regime, while no LII signal has been detected during the first 30 min of the boiler operation time. This extinction could be associated with the presence of non-incandescent particles (probably dust, fly ashes, etc.) that may absorb weakly at 1064 nm and/or scatter the light but do not induce an incandescence signal due to their large size (micrometric range). Up to 30 min, the "equivalent volume fraction" increases and reaches around 2.2 ppm.

The first LII signal is detected 35 min after the boiler operation. The extinction signal increases and the equivalent volume fraction reaches a 'plateau' region 1.5 h after the ignition. In this study, as a first hypothesis, we consider this extinction level as a background signal from non-soot particles during the total duration of the test.

When the thermal cycle is established (after 1.75 h of the boiler operation), extinction and LII signals exhibit periodic cycles linked to water temperature cycles.

The lowest concentrations of solid particles (measured by extinction) are observed when the temperature decreases and hence when no pellets are loaded in the first combustion chamber. In this region (negative slope), the extinction of the laser is probably attributed to the soot particles formed during the combustion process while the contribution of ashes via absorption or scattering is probably important in the positive slope of particles concentration regions.

The volume fraction measured by extinction was not corrected for scattering of fly ash and soot. Further experiment will include the scattering measurement perpendicular to the laser axis across the chimney. We should note that the LII measurements represent a local soot concentration detected in small volume while the extinction measurements consider all the particles present within the laser beam along the chimney diameter (120 mm).

According to the particle volume fraction measured by extinction due to soot and fly ashes, on the basis of mature soot $E(m)$ around 0.4, after the start-up phase, the LII (detected at 700 nm) trapping could reach an important value close to 70%.

In further investigation, the laser fluence will be increased to the sublimation plateau (or threshold) to minimize the

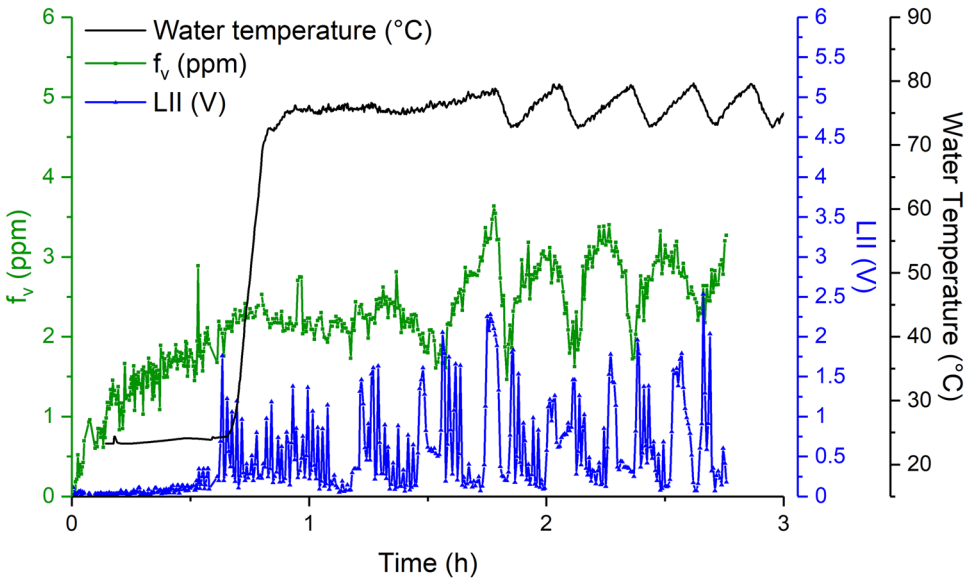

Fig. 11 Particles volume fraction (green line), broadband LII signal (blue line) and water temperature (black line) recorded simultaneously versus time

effect of laser extinction across the chimney on LII signal detection. Moreover, in future investigations the optical excess will be enlarged, to understand the influence of LII trapping and study the radial evolution of LII signal inside the chimney.

Moreover, in future investigations, to understand the influence of LII trapping, the optical excess will be enlarged to study the evolution of LII signal versus the radial position inside the chimney in the detection direction.

Finally, LII measurement using ICCD camera along the entire laser propagation will be used to ensure correct soot volume fraction measurement inside the chimney.

5 Conclusion

The aim of this study is to define an experimental protocol that provides a real-time characterization of the particulate matter emissions in a small-scale biomass boiler. The test bench used here is a 30-kW boiler fueled by wood pellets where the pellets are supplied in a fixed bed furnace by a screw conveyor. This boiler is equipped with an oxygen sensor to automatically adjust the air excess and a secondary combustion chamber that optimizes the combustion and the thermal efficiency. Laser-based diagnostics including the broadband LII, the two-color LII and the laser extinction have been performed to measure the particles volume fraction in the exhaust of the boiler. Complementary measurements of the temperature distributions in the second combustion chamber using a set of S-type thermocouples have been implemented to provide additional information about the boiler operation. Particles size distribution measurements have been carried out in the first combustion chamber and in the exhaust using a SMPS over the size range of 5–500 nm. All these measurements have been performed in the start-up, transient and steady-state phases of the boiler standard operating regime.

The experimental results can be summarized as follows:

- The flue gas temperatures measured at different positions in the second chamber show that the temperature increases when pellets are supplied in the furnace and decreases when the screw conveyor stops with maximal values reached at mid-cycle. The highest flue gas temperatures are located near the center and the top of the second chamber. The burned gases introduced into the second chamber are heated by radiation which enhances the combustion and the thermal efficiency of the boiler.
- The mean diameters of particles at the exhaust are minimal in the startup phase with a bimodal size distribution dominated by the small-size mode. Then, the particles median diameter increases significantly in the transient phase, reaches a maximum around 45 nm and then decreases slightly until reaching a plateau region around 35 nm in the steady-state regime. The particles have also a bimodal size distribution dominated by the large-size particles especially during the transient regime. In the first combustion chamber, monodisperse size distributions have been obtained during the steady state with a mean diameter of particles varying from 7 to 20 nm. Particles undergo surface growth, coagulation and agglomeration processes in the second chamber and exit the chimney with a median diameter around 35 nm.
- The broadband LII and the two-color LII techniques show that the soot concentration is very weak during the start-up phase which is consistent with the SMPS results. When the thermal cycle is established, LII emission shows periodic cycles and peaks mostly when no pellets are introduced in the first combustion chamber. In the steady-state regime, the maximal values of the soot volume fractions corresponding to the 2C-LII detection are around 160 ppb. The LII trapping along the radius of the chimney should be taken into account in further investigations.
- The laser extinction signal measured simultaneously with the broadband LII signal shows a continuous increase during the start-up regime. This suggests that the particles responsible of the laser extinction are non-incandescent particles (probably dust, fly ashes) that exceed the detection range of the SMPS (> 500 nm). When the thermal cycle is established, the extinction and LII signals exhibit both periodic cycles linked to water temperature cycles (pellets loading) and the mean particle (soot and fly ashes) volume fraction determined by extinction is around 2.2 ppm.

To correctly compare the emitted soot volume fraction by 2C-LII technique and the quantity of dust/fly ash concentration with extinction, it will be necessary in future investigations to image the LII signal over the whole diameter of the chimney using a pulsed camera.

Particles size measurements with a higher upper limit range (> 2.5 μm) should be performed to estimate the scattering contribution in the extinction measurements, elastic scattering of the laser beam which will be measured perpendicularly to the laser axis across the chimney.

The impact of the operating conditions and the pellets composition on the particulate matter emission will also be considered in the future.

Acknowledgements This work was supported by several funding sources: the Région Hauts-de-France, in the framework of the regional project SYLWATT and in partnership with LAMIH (UPHF, Valenciennes), PC2A (Lille), CCM (ULCO, Dunkerque) and Enerbiom; the company Enerbiom and the ANRT (National Association of Research and Technology) for the Ph.D. Grant awarded to Ms. Creyx; the Région Hauts-de-France for the post-doctoral grant awarded to Ms. Bejaoui.

References

1. WBA Global Bioenergy Association, n.d., WBA global bioenergy statistics 2017. https://worldbioenergy.org/uploads/WBA%20GBS%202017_hq.pdf (2017)
2. B.C. Boman, A.B. Forsberg, B.G. Järvholm, Adverse health effects from ambient air pollution in relation to residential wood combustion in modern society. Scand. J. Work Environ. Health **29**(4), 251–260 (2003)
3. M.A. Bari, G. Baumbach, B. Kuch, G. Scheffknecht, Particle-phase concentrations of polycyclic aromatic hydrocarbons in ambient air of rural residential areas in southern Germany. Air Qual. Atmos. Health **3**(2), 103–116 (2010)
4. A. Williams, J.M. Jones, L. Ma, M. Pourkashanian, Pollutants from the combustion of solid biomass fuels. Prog. Energy Combust. Sci. **38**, 113–137 (2012)
5. R. Pandey, A.K. Tyagi, Particulate matter emissions from domestic biomass burning in a rural tribal location in the lower Himalayas in India: concern over climate change. Small Scale For. **11**, 185–192 (2012)
6. S.S. Amaral, J. Andrade de Carvalho, M.A.M. Costa, C. Pinheiro, Particulate matter emission factors for biomass combustion. Atmosphere **7**, 141–146 (2016)
7. K.L. Bignal, S. Langridge, J.L. Zhou, Release of polycyclic aromatic hydrocarbons, carbon monoxide and particulate matter from biomass combustion in a wood-fired boiler under varying boiler conditions. Atmos. Environ. **42**, 8863–8871 (2008)
8. H. Liu, G. Qiu, Y. Shao, S.B. Riffat, Experimental investigation on flue gas emissions of a domestic biomass boiler under normal and idle combustion conditions. Int. J. Low Carbon Technol. **5**, 88–95 (2010)
9. K.M. Win, T. Persson, C. Bales, Particles and gaseous emissions from realistic operation of residential wood pellet heating systems. Atmos. Environ. **59**, 320–327 (2012)
10. M.M. Roy, A. Dutta, K. Corscadden, An experimental study of combustion and emissions of biomass pellets in a prototype pellet furnace. Appl. Energy **108**, 298–307 (2013)
11. L. Limousy, M. Jeguirim, P. Dutournié, N. Kraiem, M. Lajili, R. Said, Gaseous products and particulate matter emissions of biomass residential boiler fired with spent coffee grounds pellets. Fuel **107**, 323–329 (2013)
12. C. Serrano, H. Portero, E. Monedero, Pine chips combustion in a 50-kW domestic biomass boiler. Fuel **111**, 564–573 (2013)
13. W.J. Smith, S. Morrin, D.J. Timoney, Effect of operating condition on the particulate matter emission factor for a domestic biomass boiler. J. Power Energy **225**(Part A), 614–618 (2015)
14. V.K. Verma, S. Bram, F. Delattin, P. Laha, I. Vandendael, A. Hubin, J. De Ruyck, Agro-pellets for domestic heating boilers: standard laboratory and real life performance. Appl. Energy **90**, 17–23 (2012)
15. M. Markovic, E.A. Bramer, G. Brem, Experimental investigation of wood combustion in a fixed bed with hot air. Waste Manag. **34**, 49–62 (2014)
16. V. Hindasageri, R.P. Vedula, S.V. Prabhu, Thermocouple error correction for measuring the flame temperature with determination of emissivity and heat transfer coefficient. Rev. Sci. Instrum. **84**, 024902 (2013). **(1–11)**
17. L.A. Melton, Soot diagnostics based on laser heating. Appl. Opt. **23**, 2201–2208 (1984)
18. B. Axelsson, R. Collin, P.E. Bengtsson, Laser-induced incandescence for soot particle size measurements in premixed flat flames. Appl. Opt. **39**, 83–90 (2000)
19. D.R. Snelling, F. Liu, G.J. Smallwood, O.L. Gülder, Determination of the soot absorption function and thermal accommodation coefficient using low-fluence LII in a laminar coflow ethylene diffusion flame. Combust. Flame **136**, 180–190 (2004)
20. B. Axelsson, R. Collin, P.E. Bengtsson, Laser-induced incandescence for soot particle size and volume fraction measurements using on-line extinction calibration. Appl. Phys. B **72**, 367–372 (2001)
21. M.Y. Choi, G.W. Mulholland, A. Hamins, T. Kashiwagi, Comparisons of the soot volume fraction using gravimetric and light extinction techniques. Combust. Flame **102**, 161–169 (1995)
22. C. Schulz, B.F. Kock, M. Hofmann, H. Michelsen, S. Will, B. Bougie, R. Suntz, G. Smallwood, Laser-induced incandescence: recent trends and current questions. Appl. Phys. B **83**, 333–354 (2006)
23. H.A. Michelsen, Understanding and predicting the temporal response of laser-induced incandescence from carbonaceous particles. J. Chem. Phys. **118**, 7012–7045 (2003)
24. S. Bejaoui, R. Lemaire, P. Desgroux, E. Therssen, Experimental study of the $E(m, \lambda)/E(m, 1064)$ ratio as a function of wavelength, fuel type, height above the burner and temperature. Appl. Phys. B **116**, 313–323 (2013)
25. U.O. Köylü, G.M. Faeth, Spectral extinction coefficients of soot aggregates from turbulent diffusion flames. J. Heat Transf. **118**, 415–421 (1996)
26. S.S. Krishnan, K.C. Lin, G.M. Faeth, Extinction and scattering properties of soot emitted from buoyant turbulent diffusion flames. J. Heat Transf. **123**, 331–339 (2001)
27. J. Yon, R. Lemaire, E. Therssen, P. Desgroux, A. Coppalle, K.F. Ren, Examination of wavelength dependent soot optical properties of diesel and diesel/rapeseed methyl ester mixture by extinction spectra analysis and LII measurements. Appl. Phys. B **104**, 253–271 (2011)
28. E. Therssen, Y. Bouvier, C. Schoemaecker-Moreau, X. Mercier, P. Desgroux, M. Ziskind, C. Focsa, Determination of the ratio of soot refractive index function $E(m)$ at the two wavelengths 532 and 1064 nm by laser induced incandescence. Appl. Phys. B **89**, 417–427 (2007)
29. J. Zerbs, K.P. Geigle, O. Lammel, J. Hader, R. Stirn, R. Hadef, W. Meier, The influence of wavelength in extinction measurements and beam steering in laser-induced incandescence measurements in sooting flames. Appl. Phys. B **96**, 683–694 (2009)
30. J. Yon, E. Therssen, F. Liu, S. Bejaoui, D. Hebert, Influence of soot aggregate size and internal multiple scattering on LII signal and the absorption function variation with wavelength determined by the TEW-LII method. Appl. Phys. B **119**, 643–655 (2015)